SLAC–PUB–17473
September 2019

THE DIRC COUNTER: A PARTICLE IDENTIFICATION DEVICE FOR THE B FACTORY*

BLAIR RATCLIFF

Stanford Linear Accelerator Center, Stanford University, Stanford, CA 94309 USA

ABSTRACT

A design for a very thin, solid radiator, totally internally reflecting, imaging Cherenkov counter (DIRC) is described. This device is well matched to the hadronic particle identification requirements at an asymmetric e^+e^- B Factory.

1. Introduction

It is generally agreed that high quality hadronic particle identification is fundamental to the central mission of understanding CP violation at the proposed asymmetric B factories, but there is as yet no clear "consensus" solution for such a device.[1,2] As shown in Fig. 1, for a typical collider asymmetry of 9 on 3.1 GeV/c, the average produced momenta are quite soft (usually well below 1.0 GeV/c). However, efficient tagging of B mesons requires good kaon identification up to about 2.0 GeV/c, and, as shown in Fig. 2, rare but important low multiplicity processes have significant numbers of tracks with momenta above 4.0 GeV/c. Moreover, in general there is a substantial correlation of momentum and lab angle, with the fastest tracks occurring in the direction of the high energy beam. Beam crossing rates at a typical B Factory are very high, occurring about every 4 ns, while the expected trigger rates and integrated backgrounds are also rather high, and the particle identification device must be relatively fast and tolerant of backgrounds.

The particle identification problem is made more difficult by the necessity to reconstruct π^0 decays with high efficiency in the calorimeter surrounding the particle identification device. This requires a calorimeter that can reconstruct photons with energies well below 100 MeV with good resolution and efficiency. Such high quality calorimetry can be attained (e.g., by CsI crystals), but such devices cost a great deal per unit volume, and the cost scales approximately as the inner radius squared. Moreover, the mass before the calorimeter must be small and well distributed to avoid compromising the performance. Studies indicate that in order to achieve the desired energy resolution in the calorimeter,

* Work supported by Department of Energy, contract DE-AC03-76SF00515. Original BaBar note 92 (1992).

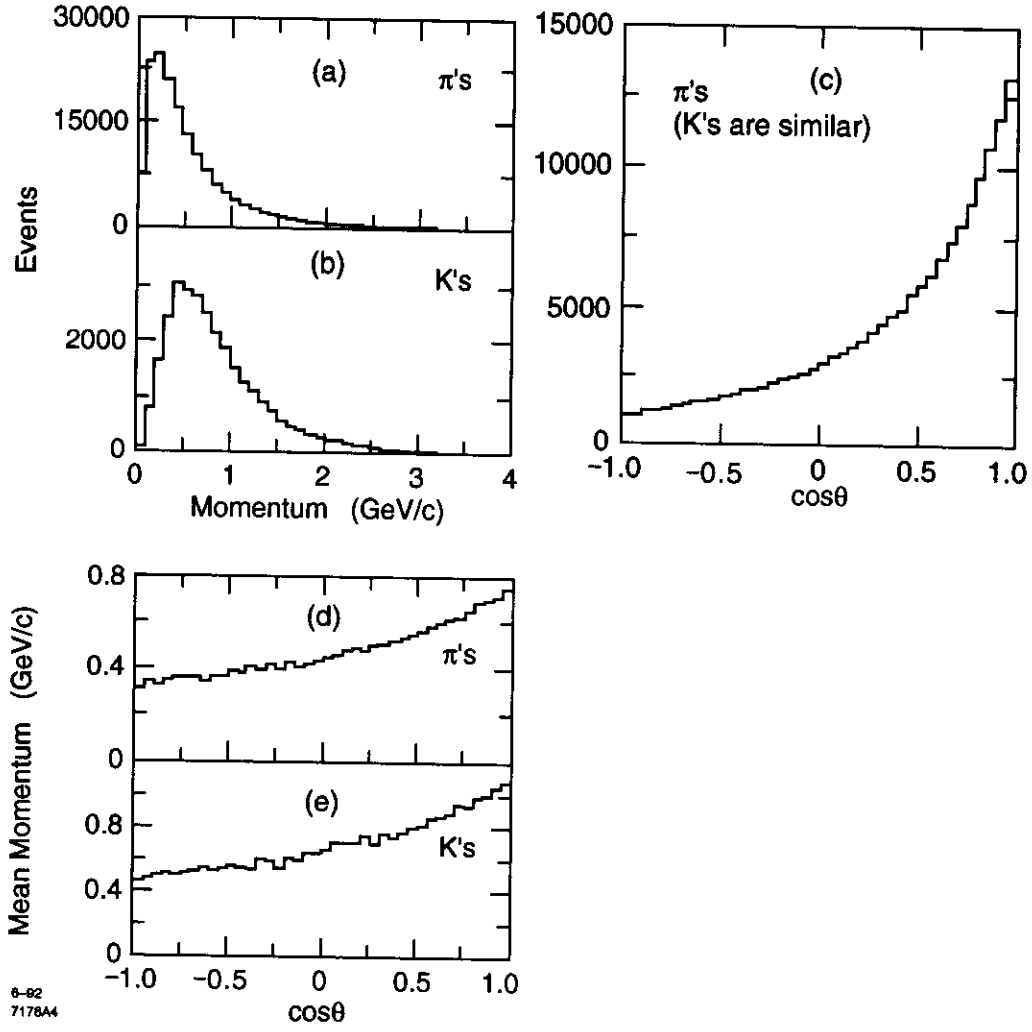

Figure 1. Distributions in momentum and laboratory angle for all pions and kaons produced in B meson decays for beam energies of 9 on 3.1 GeV/c: (a) momentum distribution for pions, (b) momentum distribution for kaons, (c) angular distribution for pions, (d) distribution of the average momentum versus the cosine of the angle for pions, (e) distribution of the average momentum versus the cosine of the angle for kaons.

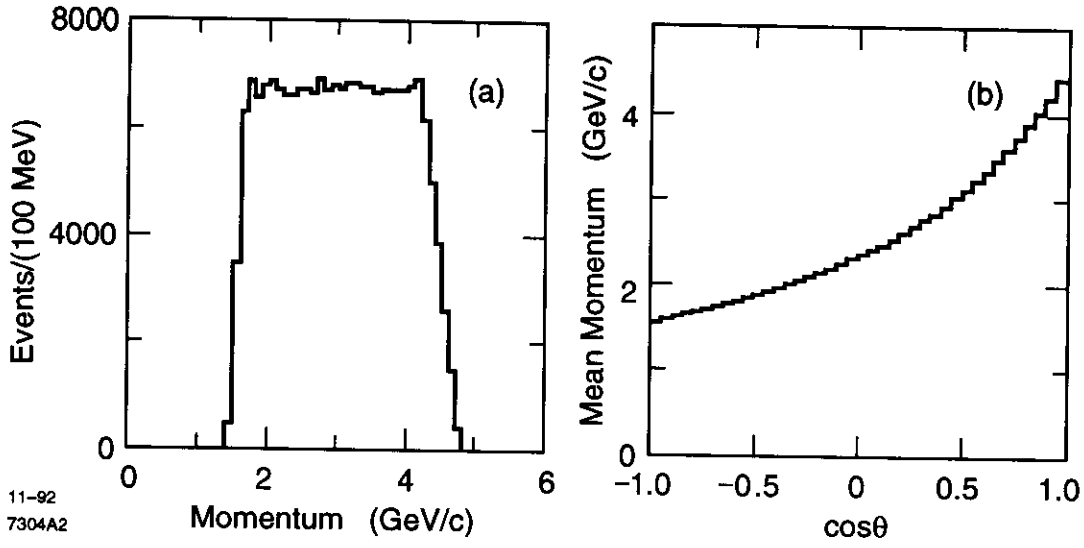

Figure 2. Distributions in momentum and laboratory angle for B —> $\pi^+\pi^-$ produced by beam energies of 9 on 3.1 GeV/c: (a) momentum distribution, (b) average momentum versus the cosine of the laboratory angle.

every effort must be made to keep the material in front of the calorimeter below about 10–15% of a radiation length; and, in general, the material should be as close to the calorimeter as possible in order to avoid losing the photons altogether when conversion electrons curl up in the magnetic field.[3]

A number of particle identification strategies have been proposed for coping with this difficult environment, and active R&D is underway on many of these options.[4] In this note, we describe a new kind of imaging Cherenkov counter that, in principle, allows very high quality particle identification to be performed up to the maximum B Factory momentum in about 2–3 cm of radial space.

2. THE DIRC IMAGING PRINCIPLE

In proximity focused, imaging Cherenkov counters of the RICH or CRID type, the light from the radiating medium emerges from the thin radiator and expands in a "cone" which approximately encircles the particle trajectory. The detector lies in the particle's path and must be placed sufficiently far away that adequate angular resolution for each photon can be attained; i.e., the thickness of the radiator must be much smaller than the stand-off distance. This implies a certain minimum thickness (typically 15–20 cm) for the total detector. Since both radiator and detector lie in the particle path, it is difficult to reduce the material in front of the calorimeter much below 15%. In general, only a portion of the light emerges from the radiating medium and can be imaged. The remainder is totally internally reflected inside the radiator and lost–the fractional amount becoming larger as the index of refraction of the radiating material increases. In the device described below, we "invert" the usual CRID (or RICH) imaging approach–using only these internally reflected photons to form the Cherenkov image. We call this device the DIRC (Detection [of] Internally Reflected Cherenkov [light]) counter.

3. THE DIRC IMAGING PRINCIPLE

The geometry of a single radiator of the DIRC is shown schematically in Fig. 3. Each radiator is a long, thin, flat "bar" with rectangular cross section $[t_x, t_y]$. There is a photodetection surface positioned some distance (l) away from the end of the bar. A track with velocity β passing through the radiator with refractive index n_1 emits Cherenkov radiation in a cone around the particle trajectory with cone half angle θ_C given by the Cherenkov relation

$$\cos\theta_C = \frac{1}{n_1\beta}. \qquad (1)$$

The angles, positions, and momentum of the track are provided by a tracking device located in front of the radiator. If the index of refraction of the radiating material (n_1) substantially exceeds $\sqrt{2}$, and n_3 is approximately 1, then, for a particle close to $\beta = 1$, some portion of the light will always be transported down the "bar" to the end. Since the radiator cross-section is rectangular, angles are maintained in reflections at the surfaces of the bar (up

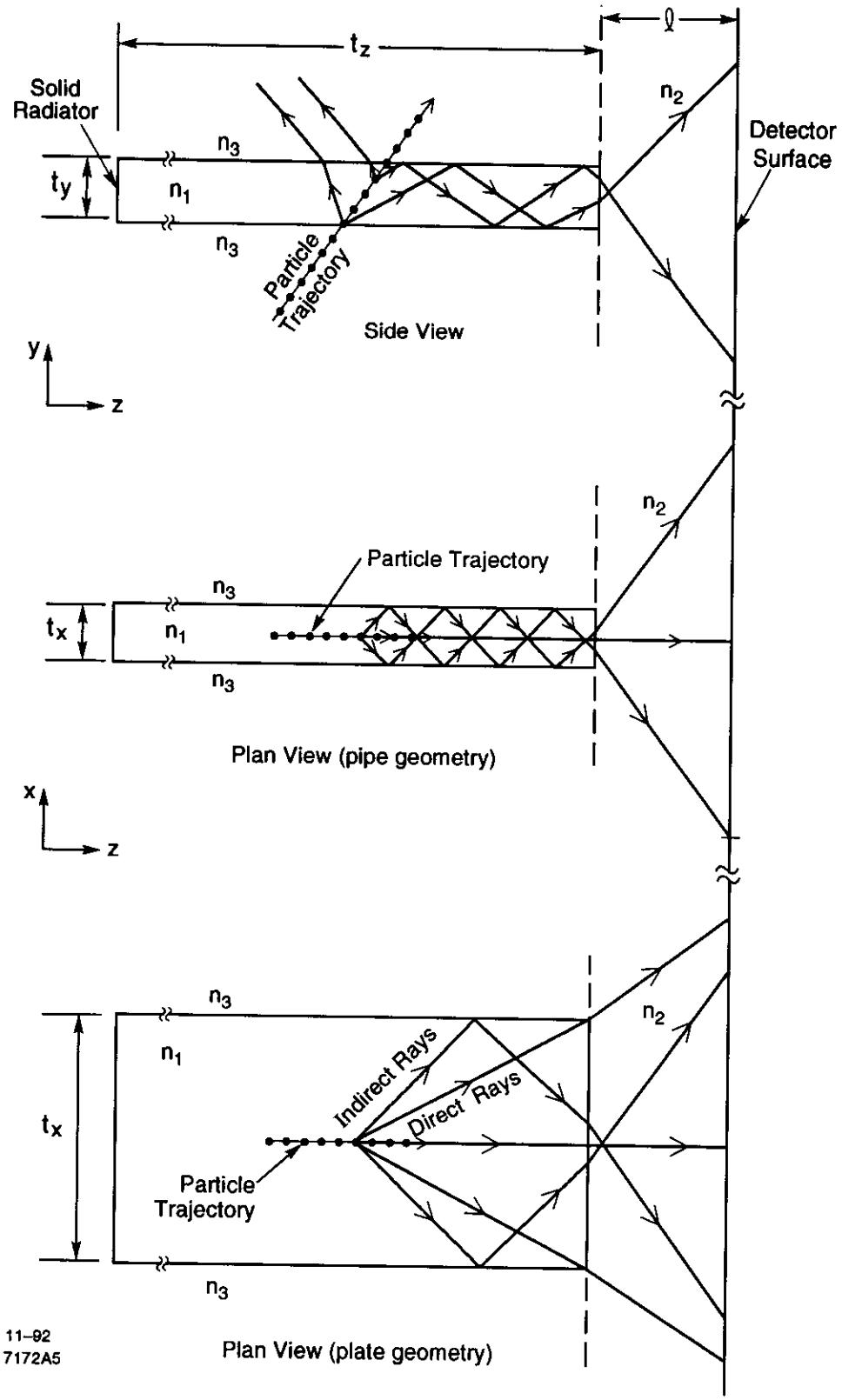

Figure 3. Schematic of a radiator bar of the DIRC counter for two different radiator widths (pipe and plate) described in the text; the particle trajectory is shown as a line connected by dots; representative trajectories of Cherenkov photons are shown by lines with arrows.

to an additional up-down/left-right ambiguity). Thus, in a perfect bar, the portion of the Cherenkov cone that lies inside the total internal reflection angle is transported undistorted down the bar to the end. When it reaches the end, the light either reflects or emerges into a standoff region with index n_2. It then travels some distance until it hits a two dimensional detection surface, where it forms an image on the surface as shown in Fig. 4. The image is essentially a conic section of the cone–suitably modified by refraction at the n_1, n_2 interface. It has been "doubled" because of the up-down reflection ambiguity. In the case shown, the track enters the radiator in the y-z plane so that the left and right going images are symmetrical. Since the locus of the image depends on the polar and azimuthal Cherenkov angles (θ_C, ϕ_C), particle identification using Cherenkov angular information can proceed using essentially the same hypothesis testing techniques employed by imaging Cherenkov devices of the RICH/CRID type.[5]

Two different image loci are shown in Fig. 4 corresponding to different extremes for the width (t_x) of the bar, as shown schematically in Fig. 3. In one limiting case, called the PLATE geometry, the bar is sufficiently wide that no reflections occur from the sides of the bar, and there is no left-right imaging ambiguity. That is, the "indirect" rays shown in Fig. 3 do not emerge from the end. In the other limit, the PIPE geometry, the bar width t_x is much smaller than the photon measurement resolution, and there is complete left-right overlap.

The PLATE geometry has fewer ambiguities in the case where it is geometrically feasible to make the plate very wide (perhaps in a fixed target environment), but it does not seem possible to devise a full acceptance counter for a solenoidal detector at a collider without a significant number of photon bounces from the sides. Unless the PLATE has a large width/length ratio, the image depends in detail on the number of bounces, the width of the radiator, the position of the track in the radiator bar, etc., and consists of a number of disconnected pieces as shown in Fig. 5. These individual pieces can themselves overlap and provide significant ambiguity, although some of the ambiguities may be removed using the timing dimension. In any case, it appears simplest to accept the left/right imaging ambiguity implied by the PIPE geometry, as we will do in the remainder of this paper. Then, in the limit of infinite transmission coefficient and small pipes, the observed image is dependent only on the track velocity and angles with respect to the bar, and independent of position in the bar.[6]

Not all Cherenkov photons produced in the radiator can be collected by the detector. Consider, for example, a $\beta = 1$ track penetrating a radiator bar in the y–z plane in a geometry like that above, in a simple model where the internal absorption coefficient is 0.0, and where the internal reflection coefficient is 1.0 for total internal reflection and 0.0 elsewhere. Figure 6 shows the fraction of produced Cherenkov photons which hit the detector as a function of dip angle. The average fraction of photons which penetrate the end is only about 30% even with the unrealistic assumption that photons which emerge at very large angles are efficiently transmitted through the end. Clearly, if reflections from the end surface are properly accounted, the fraction is even less. Even more troublesome is the fact that near $\theta_D=0^o$ (i.e., near perpendicular track incidence) the fraction of photons which can be imaged drops essentially to 0.

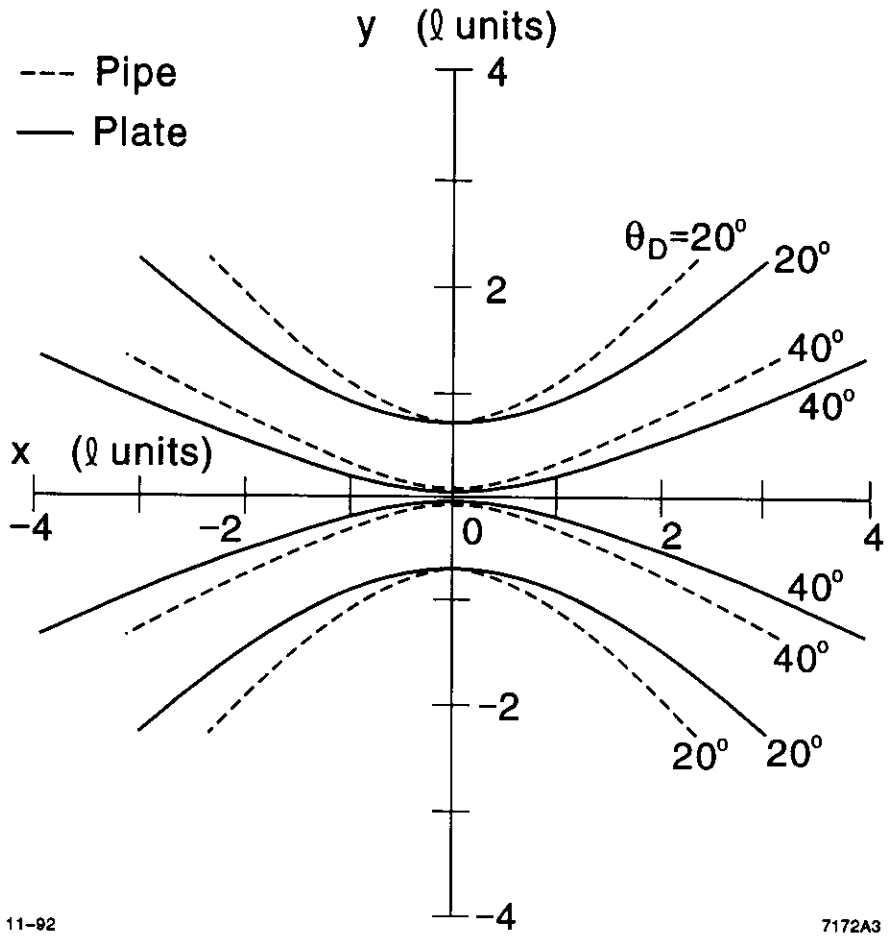

Figure 4. Loci of images for a $\beta = 1$ track at two different track dip angles produced by a single radiator of a DIRC counter on a planer surface placed at distance ℓ from the end of the radiator, in the zero thickness (t_y) limit. The track azimuthal angle (dx/dy) is zero. The refractive indices of the radiator and the detector standoff regions are n_1=1.474 and n_2=1.0, respectively. The dashed and solid lines correspond to different limits on the width (t_x) discussed in the text.

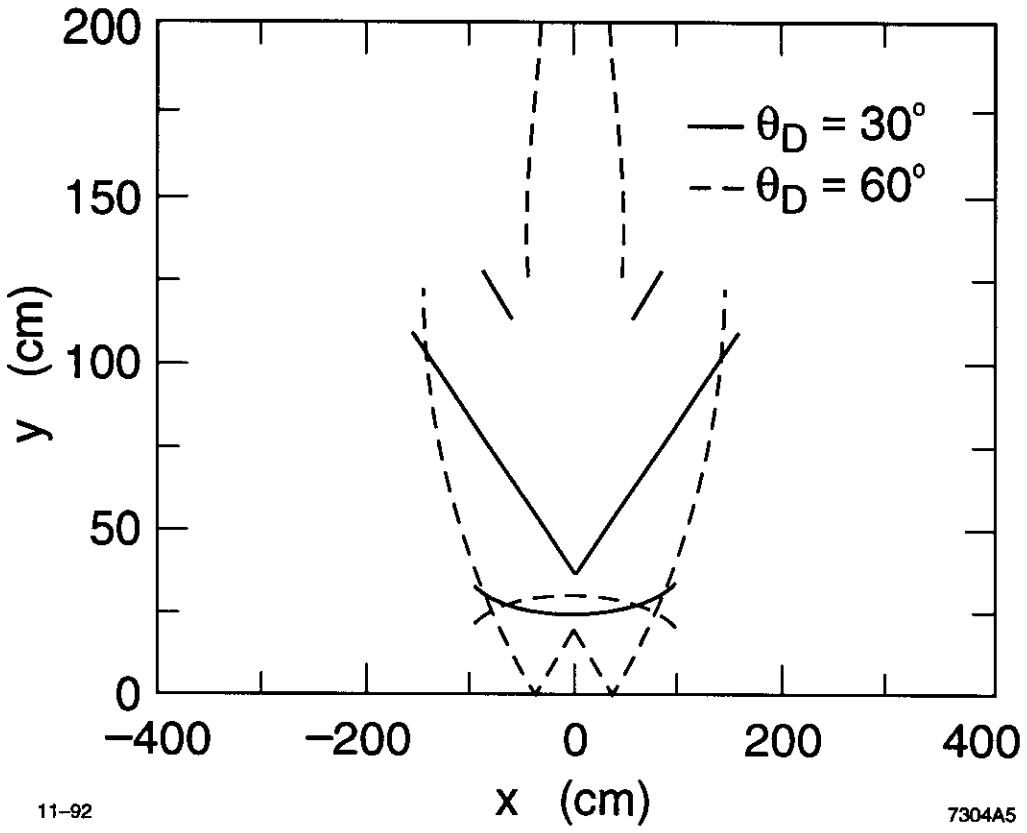

Figure 5. Loci of images for a $\beta = 1$ track for $\theta_D = 30^o$ (solid line) and $\theta_D = 60^o$ (dashed line) produced by a single radiator of a DIRC counter on a planer surface 100 cm from the end of the radiator, in the zero thickness (t_y) limit. The plate width (t_x) is 100 cm. The track penetrates the plate 100 cm from the end with an azimuthal angle of zero. These images are reflected at the $y = 0$ axis. The refractive indices of the radiator and the detector standoff regions are n_1=1.474 and n_2=1.0, respectively.

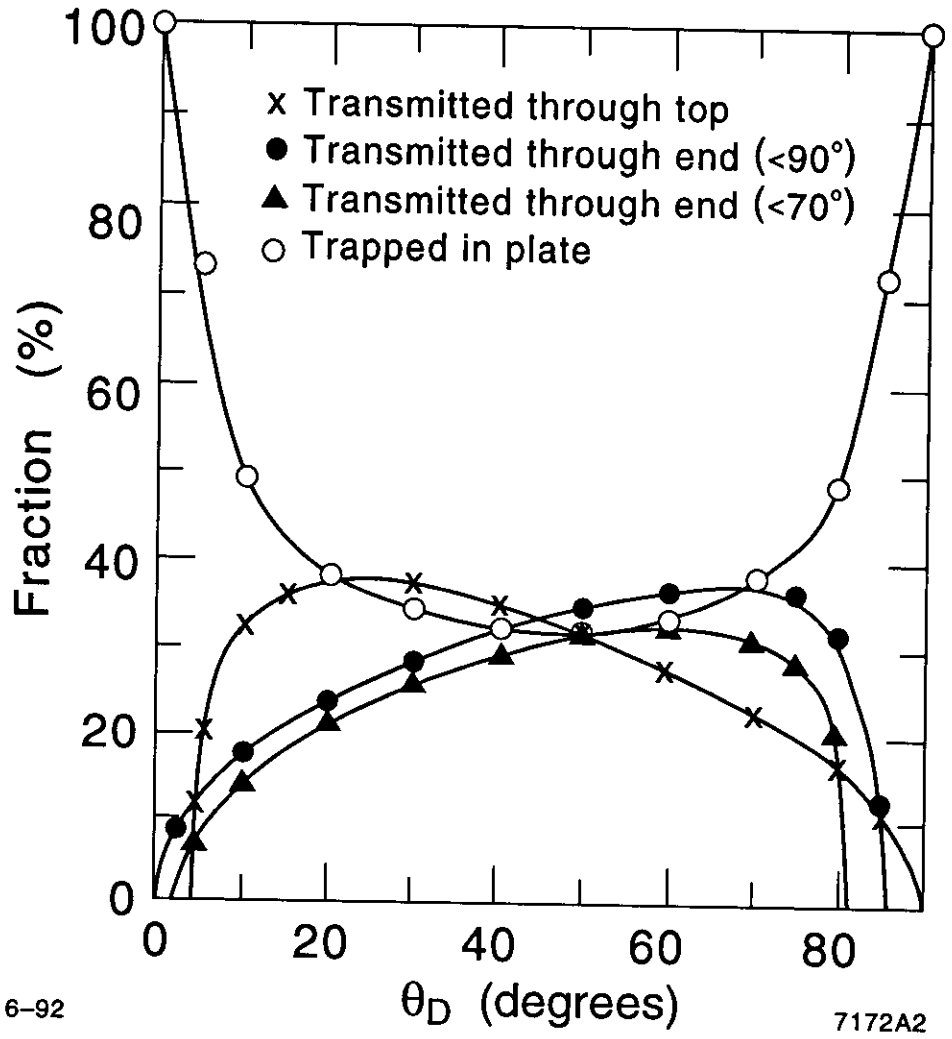

Figure 6. The fraction of Cherenkov photons transmitted to the detector (solid points) as a function of dip angle θ_D for a $\beta = 1$ track in the simple model described in the text. The refractive indices of the radiator and the detector standoff regions are $n_1 = 1.474$ and $n_2 = 1.0$, respectively. The solid circles include photons emitted at all angles whereas the solid triangles include only those photons which leave the surface with an angle of less than 70^o with respect to the surface normal. The crosses show the fraction transmitted through the radiator top surface, which would be useful in a detector of the RICH/CRID type. The open circles show that a substantial number of Cherenkov photons are trapped in the plate.

However, if the region at the radiator end is filled with a material with the same index as the radiator (i.e. $n_1=n_2$), then the images will emerge without reflection or refraction at the end surface. Figure 7 shows the Cherenkov photon transport efficiency as a function of track β in this case. There are two distinct cases, corresponding to track dip angles lying either above or below the internal reflection limit of 47.3°. For the first case, the minimum transmission occurs at β =1, is maximum at Cherenkov threshold, and exceeds 60% for all particle velocities above the Cherenkov threshold; for the second, the maximum transmission occurs at β =1, and falls to zero below a cutoff β which lies above the Cherenkov threshold. In any case, the nominal transmission exceeds 45% for all angles when β exceeds 0.93, which corresponds to P_π =0.35, and P_K=1.24 GeV/c. Below 1.24 GeV/c, a DIRC with these parameters will function as a threshold Cherenkov for π/K separation over the central part of the angular acceptance, and will be unable to distinguish kaons from protons there.

4. THE RADIATOR

For a solenoidal geometry, the radiators must have very long Cherenkov photon absorption length and high quality surface finish (for good transmittance down the bar); flat, orthogonal surfaces (for accurate image transmission); low chromatic dispersion (to allow a good measurement of the Cherenkov angle); appropriate index of refraction (to transmit light down the bar); and preferably, long radiation length. Though a short device could be built using one of the fluoride glasses (e.g., LiF or CaF_2) operating in the TMAE regime, we know of no material suitable for operation of a long device (e.g., 2–6 m) in the 1700–2000 A° region where TMAE is sensitive. The "obvious" radiator choice for a long device is quartz, working in the visible to near UV range (i.e., 3000-6000 A°). As shown in Fig. 8, it has a transmission length which exceeds 50 m over most of this wavelength range; takes a high quality polish so that internal reflection coefficients can be made high; has the lowest dispersion of the oxide glasses (Abbe number 67.8); and can be procured in large pieces at relatively modest cost.

Optical plastics typically have similar indices of refraction and much longer radiation lengths (about a factor of three better than oxide glasses). Therefore, they could be a factor of three thicker, and the manufacturing tolerances and absorption length requirements are substantially less severe. Even though shrinkage probably does not allow pieces to be molded, plastics are easily machined, and might very well be substantially cheaper to produce than quartz bars. It is unclear if adequate surface polish could be easily attained on the machined surfaces. Unfortunately, transmission lengths in the 3000-4500 A° regime are very much shorter than those of quartz and tend to be batch dependent as well. Given that the number of Cherenkov photons peaks like $1/\lambda^2$, the performance of a device with a very long plastic radiator is probably marginal. Plastic could be useful for a shorter device and does deserve further study as well to understand if the internal transmittance might possibly be improved.

The radiator matching material between the detector and the radiator bar should be well matched in refractive index to the radiator and should have a rather long absorption length.

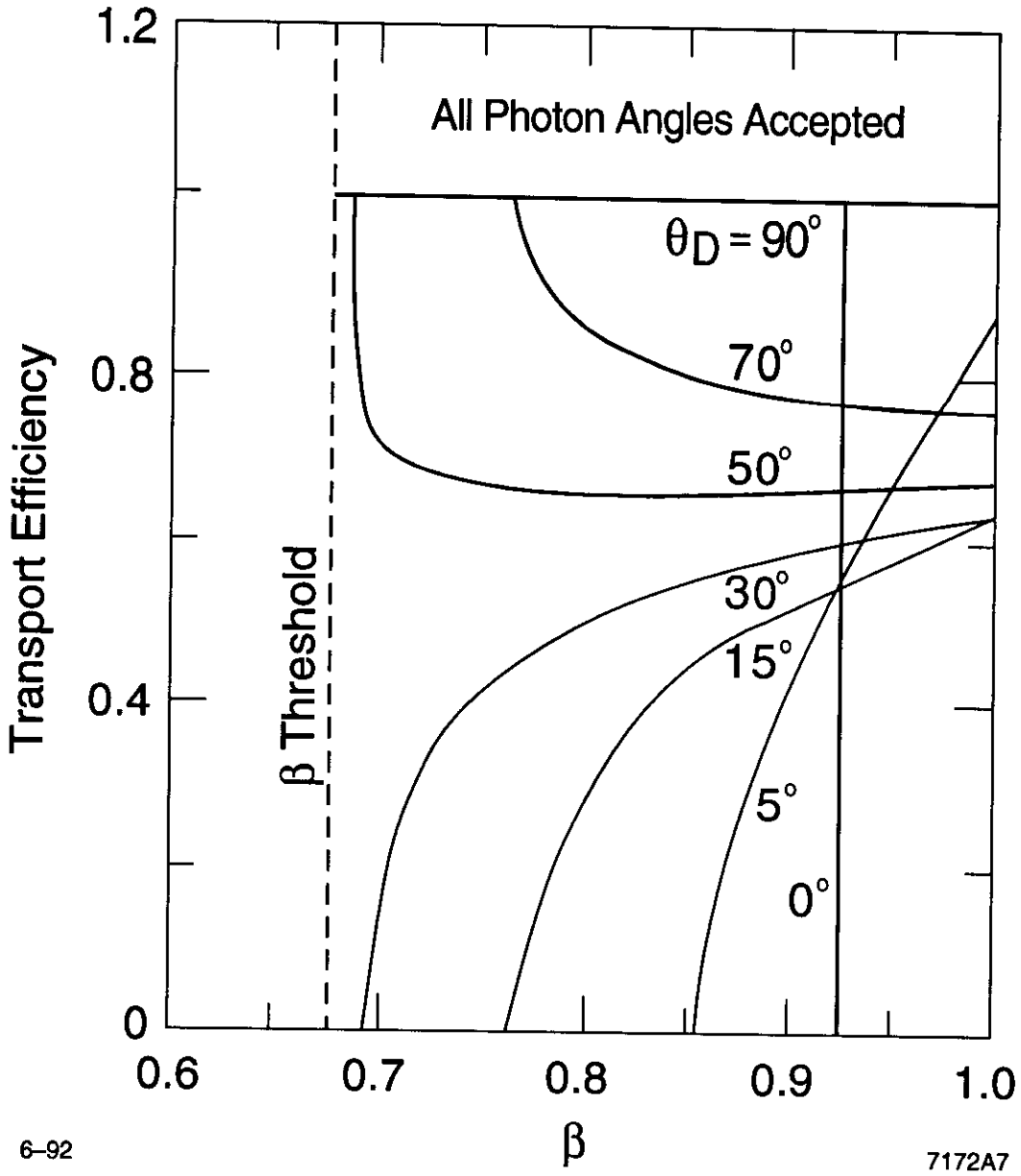

Figure 7. The fraction of Cherenkov photons transmitted to the detector as a function of β in the simple model described in the text. The refractive indices of the radiator and the detector standoff regions are equal.

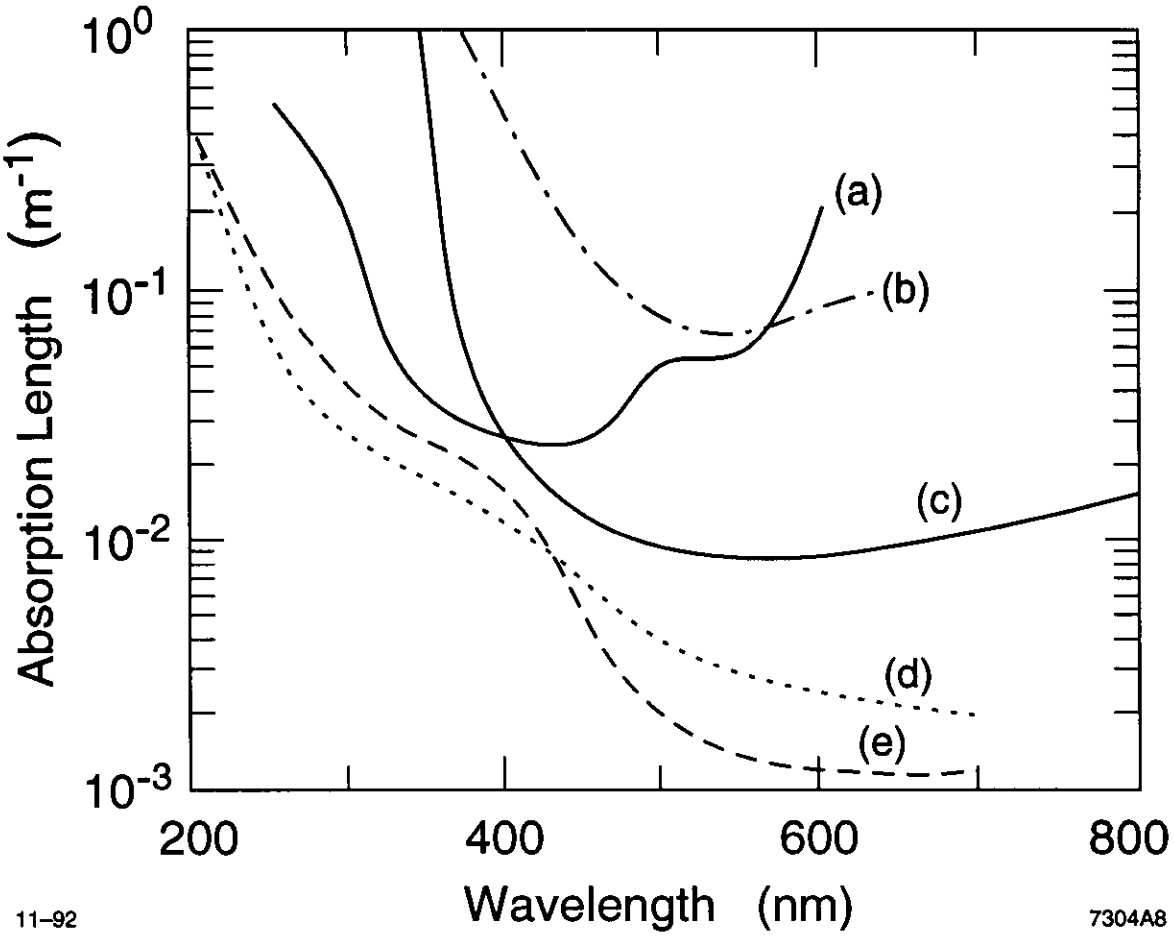

Figure 8. Examples of absorption lengths as a function of wavelength for some potential radiator and standoff region materials: (a) water (IMB quality),[7] (B) UVT acrylic,[8] (c) laser liquid 3421,[9] (d) fused silica fiber,[10] (e) bulk fused silica.[11]

If an optical plastic were chosen for the radiator, it might be feasible to cast the standoff region from the same plastic. However, in the case of quartz, it seems more likely that the region would be filled with a liquid. Though there are liquid materials available which match the refractive index of quartz extremely well, their transmission in the near UV tends to be inadequate. No exhaustive search has been undertaken, but Fig. 8 shows the response of two candidate liquids which do have reasonable UV transmissions, curves (b) for water [n_2 =1.34], and (c) for Cargille labs laser liquid 3421 [n_2 =1.41]. Water is inexpensive and quite transparent over the required range but would lead to some modest reflective losses at the n_1,n_2 interface for large angles. Liquid 3421 has a somewhat better refractive index match but cuts off earlier in 3000-4000 A° range, which would reduce the effective N_0.

For the rest of this paper, we will assume that the radiator bars are made of quartz with index of refraction n_1=1.474, when weighted by the Cherenkov spectrum and the photodetector response, and for simplicity will also assume that $n_1 = n_2$.

5. THE PHOTODETECTOR

The number of Cherenkov photons produced and transmitted to the detector surface is generally small, so it is important to obtain good efficiency from the photodetector. Moreover, since the position of each photon must be detected, the single photon signal-to-noise ratio must be very good. The photodetector surface must sit some minimum distance away from the radiator end (to obtain adequate resolution) and must therefore be rather large. Finally, the detector should be rather fast. The "classic" device which fulfills these conditions is the photomultiplier tube, and a photodetection surface can be made of an array of these tubes. A photomultiplier is modestly efficient for single photoelectrons, has extremely good signal-to-noise, is very fast, and can cover large areas at modest cost. The packing fraction in a closely packed array is typically about 66%. In principle, the collection efficiency can be improved with a optical collection system, but in practice, given the large angular acceptances involved, it is unclear if a substantial improvement can actually be obtained. In the future, substantially higher quantum efficiencies might be obtained with silicon devices,[12] but single photon performance in the visible range has only been demonstrated with very cold devices.[13] For definiteness in the remainder of this paper, we will assume that the photodetector is made of a closely packed photomultiplier array.

This has the conceptual "advantage" that the detector uses completely "conventional" technology whose performance is well understood and can presumably be reliably simulated. Such a detector is also self-triggering and very fast. Not only does it allow reliable tagging of beam crossings (which are about 4 ns apart), but it should also be a very good TOF counter. Unlike the typical scintillation device, each photon which converts is timed and its path length in the bar is well known (since its Cherenkov angles and emission points are measured), so the TOF resolution should improve like the $\sqrt{N_{PE}}$, and the resolution should be well under 100 ps in most cases. The timing resolution will also provide modest spatial resolution (~ 10 cm for a typical PMT) along the bar, and can be used to separate the direction of the photon if a reflective surface has been used on one end. Alternatively, the timing provides a measure of the photon path length to the photodetector.

Since this depends on the light propagation angles, and production point in the bar, it provides an independent measure of a particular convolution of the Cherenkov angles, which might be useful to improve the angle measurement in some cases.

On the other hand, there are several practical "disadvantages" of phototubes. The number of phototubes required is large; there are many independent channels; and, if conventional (non-mesh) phototubes are used (mesh tubes do not have good single photoelectron performance), dealing with the magnetic field will be troublesome.

Mesh phototubes provide substantial immunity to magnetic fields. However, presently available tubes do not have very good performance in the single photoelectron regime. Their cathode sensitivity is generally about 60% of a good conventional tube, and they do not have a good single photoelectron peak. As an estimate, they might be expected to provide about 50% of the photoelectrons observed by a good conventional tube.

6. MODEL FOR B FACTORY DETECTOR

In this section, we will describe a particular model of a B factory detector which incorporates a DIRC. Many of the geometrical details of such a detector are somewhat arbitrary and a great many different models are clearly possible. However, it is hoped that by discussing a specific choice, we can illuminate some of the trade-offs implicit in the design.

A view of the forward quadrant of this "model" B Factory detector is shown in Fig. 9. In order to bypass the difficult problem of keeping the end plate masses low in the central tracking devices, the particular geometry shown has no end caps. This also allows very uniform calorimetry and the simplest possible DIRC geometry. The "stretched" geometry is particularly attractive in this case because the inner radius of the calorimeter is so small. It is assumed that the DIRC radiator consists of 1.23 x 4.0 x 560 cm (t_x, t_y, t_z) quartz bars. Each bar is read-out on only one end. There is a reflecting surface on the other end. Every other bar penetrates the iron end plate on one end. The iron-to-space ratio in the pole piece of about 1-to-1. The radiator is 10% L_{RAD} thick radially and takes up to about 2.5 cm of radial space in all. The bars are placed on a 20 sided polygonal surface, as viewed from the end of the detector, and cover about 98% of the azimuth. The detectors are closely packed arrays of conventional photomultiplier (PMT) tubes at each end. As shown in Fig. 9, the surface is a cylindrical section in elevation and approximately toroidal as viewed from the end. The detector boxes have reflecting surfaces at the inner polygonal surface (approximately in the radiator x–z plane) and at $\tan^{-1}dy/dz = 1$ to save phototubes. They are filled with a fluid whose refractive index matches that of quartz, so there are no reflections at the radiator ends or phototube windows. The device works in the near ultraviolet and the visible. It is thin and compact, robust, very fast, and self triggering.

The loci of Cherenkov images on a cylindrical detector surface for $\beta = 1$ tracks at a number of different dip angles are shown in Fig. 10 for the case where the track enters the radiator bar perpendicularly in azimuth ($\eta = 0$). The images are scaled for a standoff distance of 100 cm. Distortions in the image due to wrapping the detection cylinder around the beam pipe are neglected. The images at the detector for a particular dip angle ($\theta_D = 30^o$)

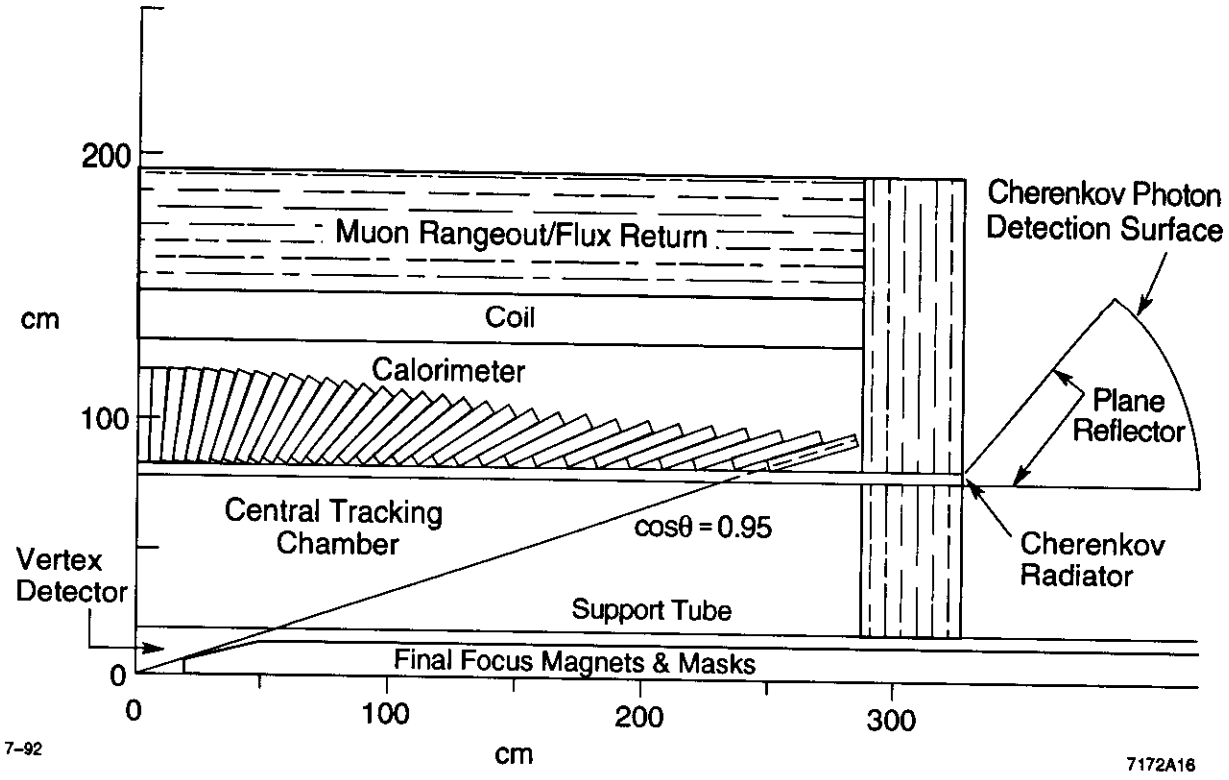

Figure 9. Schematic view of one quadrant of a B factory detector incorporating a DIRC.

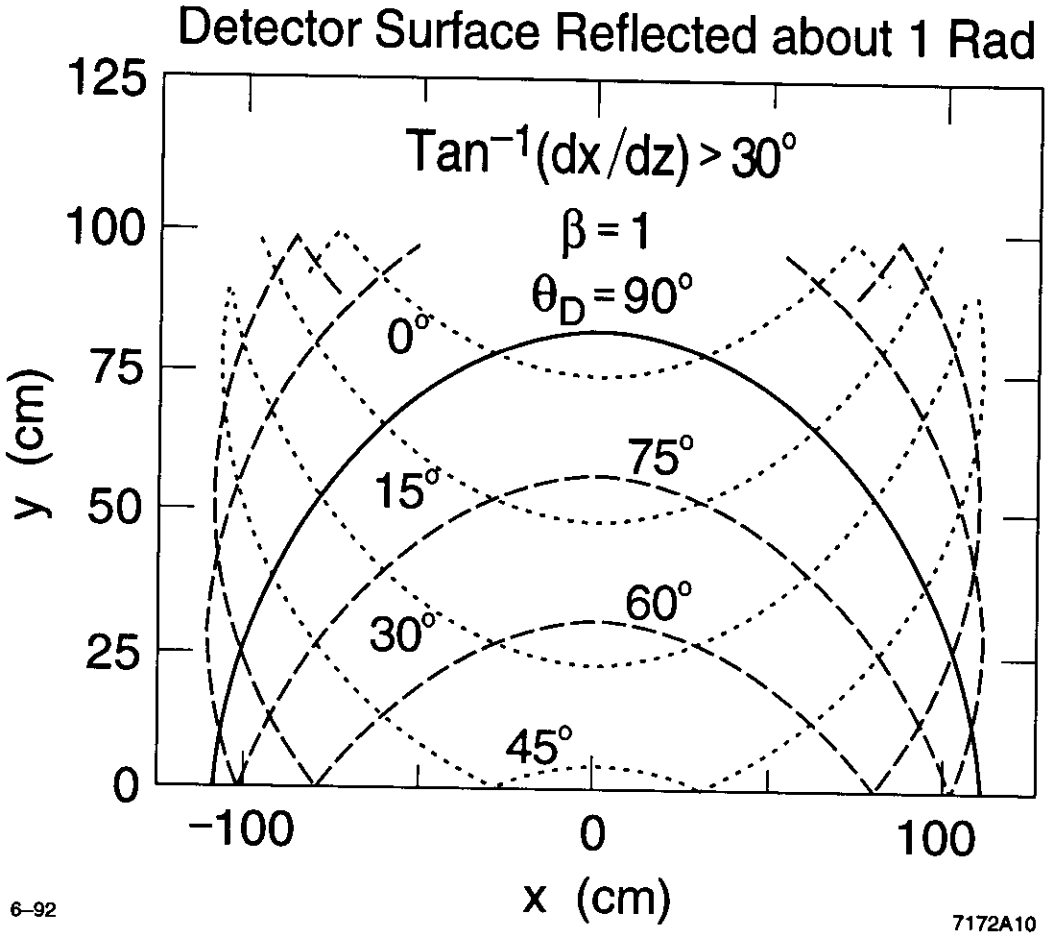

Figure 10. Loci of Cherenkov images from a $\beta = 1$ track on a cylindrical detection surface 100 cm from the radiator end. The track enters the radiator perpendicularly in azimuth. The detector surface is reflected at both 0 and 1 radians, and photons traveling down the bar with angles less than 30° are neglected.

are shown in Fig. 11 for three different angles in azimuth. For η angles other than zero, the images are "doubled" due to the side edge reflection ambiguity.

Image separation in this device occurs in the angles and in time (which can be translated into a z separation along the bar), but there is no spatial ring separation due to x, y, z location inside a given bar. In particular, the image locus is a function of the Cherenkov angles which is, of course, what allows the particle velocity to be measured. Figure 12 shows the expected separation between loci of the π/K/p images as scaled for a standoff distance of 100 cm for a 2 GeV/c track. The statistical power of the measurement is determined by the size of this separation, the relative error of each point, and the number of Cherenkov photons detected.

7. SIMPLE PERFORMANCE MODEL

In this section, we will discuss a simple model for the performance of a DIRC counter such as that described above to elucidate some of the important issues which determine the performance. The number of photoelectrons (N_{PE}) produced in the photodetector can be written as:

$$N_{PE} = \frac{\varepsilon N_0 L \sin^2\theta_C}{\cos\theta_D} \quad . \tag{2}$$

where N_0 is the Cherenkov quality factor (about 100 cm^{-1} for a good bialkali phototube), L is the radial radiator thickness ($L = t_y = 1.23$ cm), and ε is the total collection efficiency. $\sin\theta_c$ for a $\beta=1$ particle in quartz equals 0.735. ε can be thought of as being composed of two main pieces. The first is the geometrical photon transport efficiency down the bar to the photodetector. This efficiency is a strong function of track dip angle and the azimuthal acceptance for photons in the bar. As shown in Fig. 13, if the propagation efficiency is taken to be 100% for tracks with $\tan^{-1}$ dx/dz and $\tan^{-1}$ dy/dz greater than 30°, and 0% elsewhere, the efficiency varies from about 0.4 to 1.0 above a threshold in β that is dependent on the dip angle. The efficiency is also a function of track position and photon angles in the bar due to absorption and internal reflection coefficients. For simplicity in this discussion, we will assume that the radiator is very transparent and well polished so that these particular losses are small. The other large contribution to ε comes from the fact that the effective coverage of the detection surface with photocathode material is less than 1. For example, as discussed above, closely packed PMTs only cover about 66% of the surface with an active photocathode, and it is difficult to increase the efficiency much by collection optics given the large acceptance requirements.

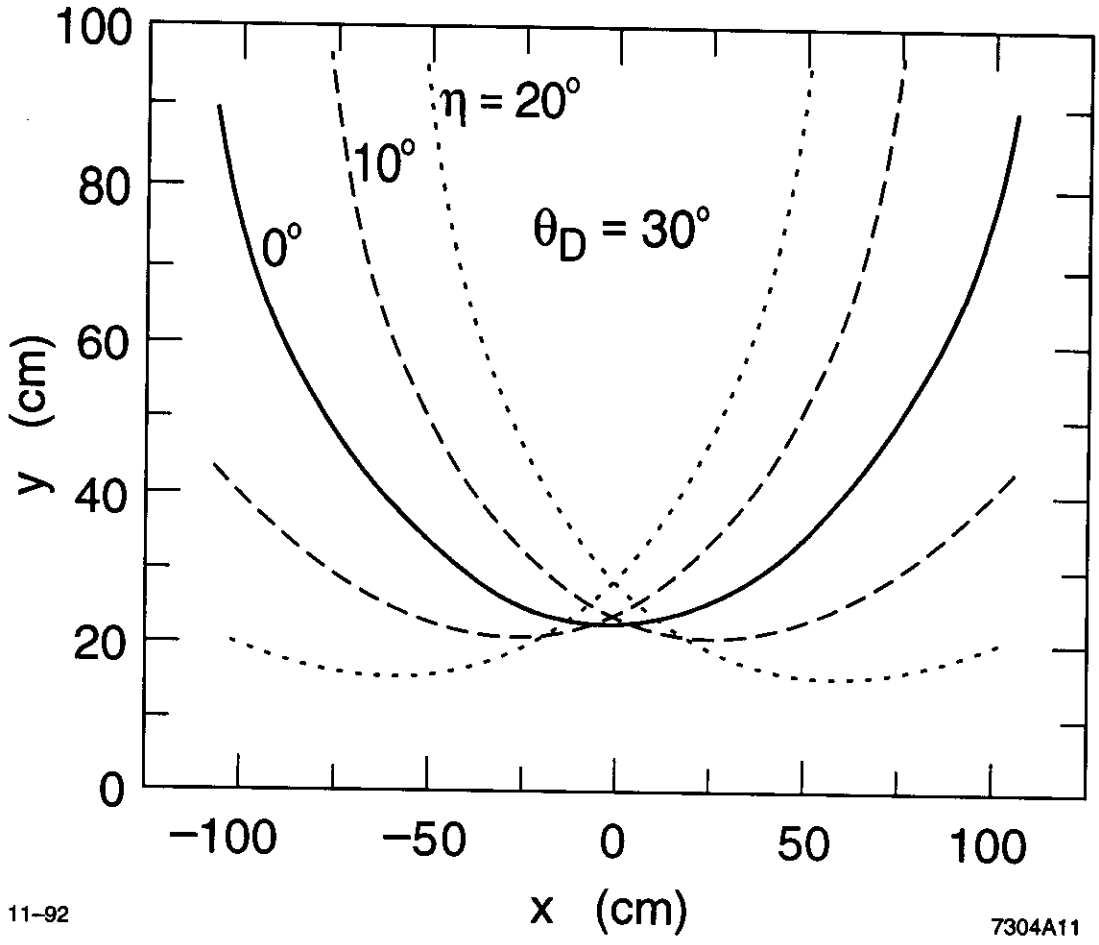

Figure 11. Loci of Cherenkov images from a $\beta = 1$ track on a cylindrical detection surface 100 cm from the radiator end. The track is at a dip angle (θ_D) of 30° and images are shown for three different azimuthal angles (η). The detector surface is reflected at both 0 rad. and 1 rad., and photons traveling down the bar with angles less than 30° are neglected.

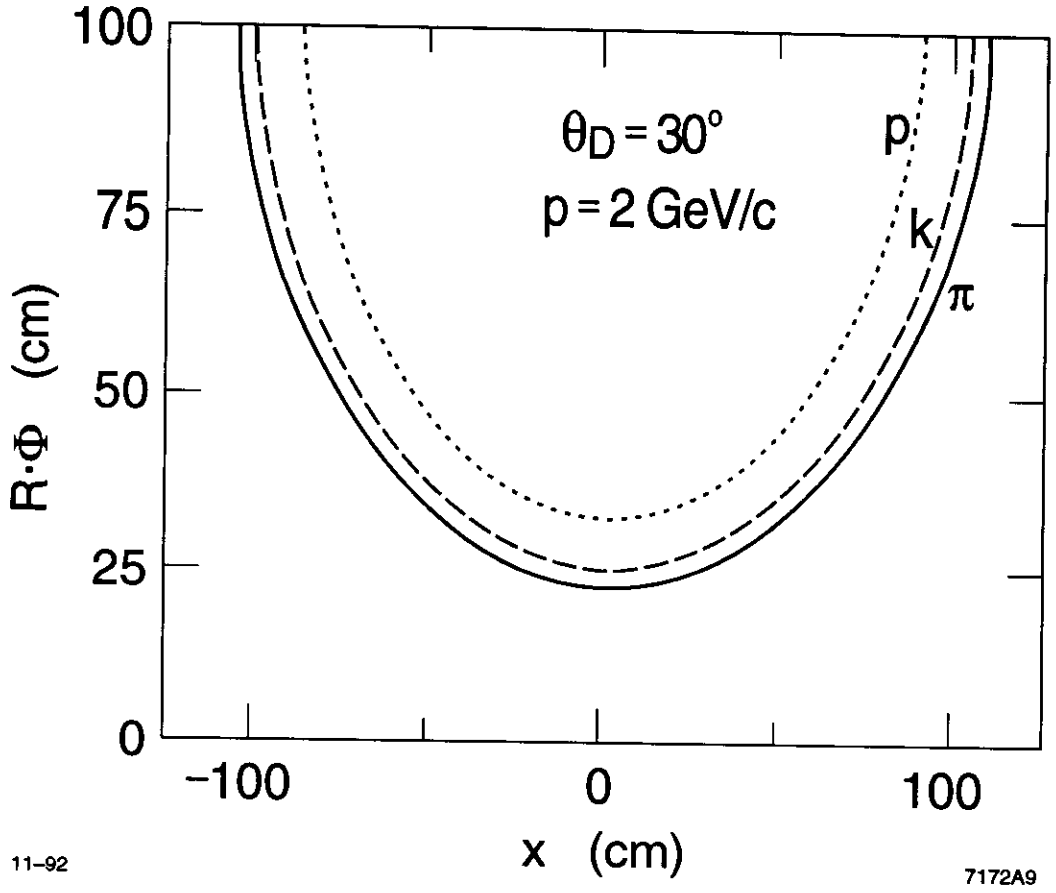

Figure 12. A comparison of the loci of Cherenkov images from π/K/p 2.0 GeV/c tracks on a cylindrical detection surface 100 cm from the radiator end. The tracks are at dip angles (θ_D) of 30° and azimuthal angles (η) of zero. The detector surface is reflected at both 0 and 1 rad., and photons traveling down the bar with angles less than 30° are neglected.

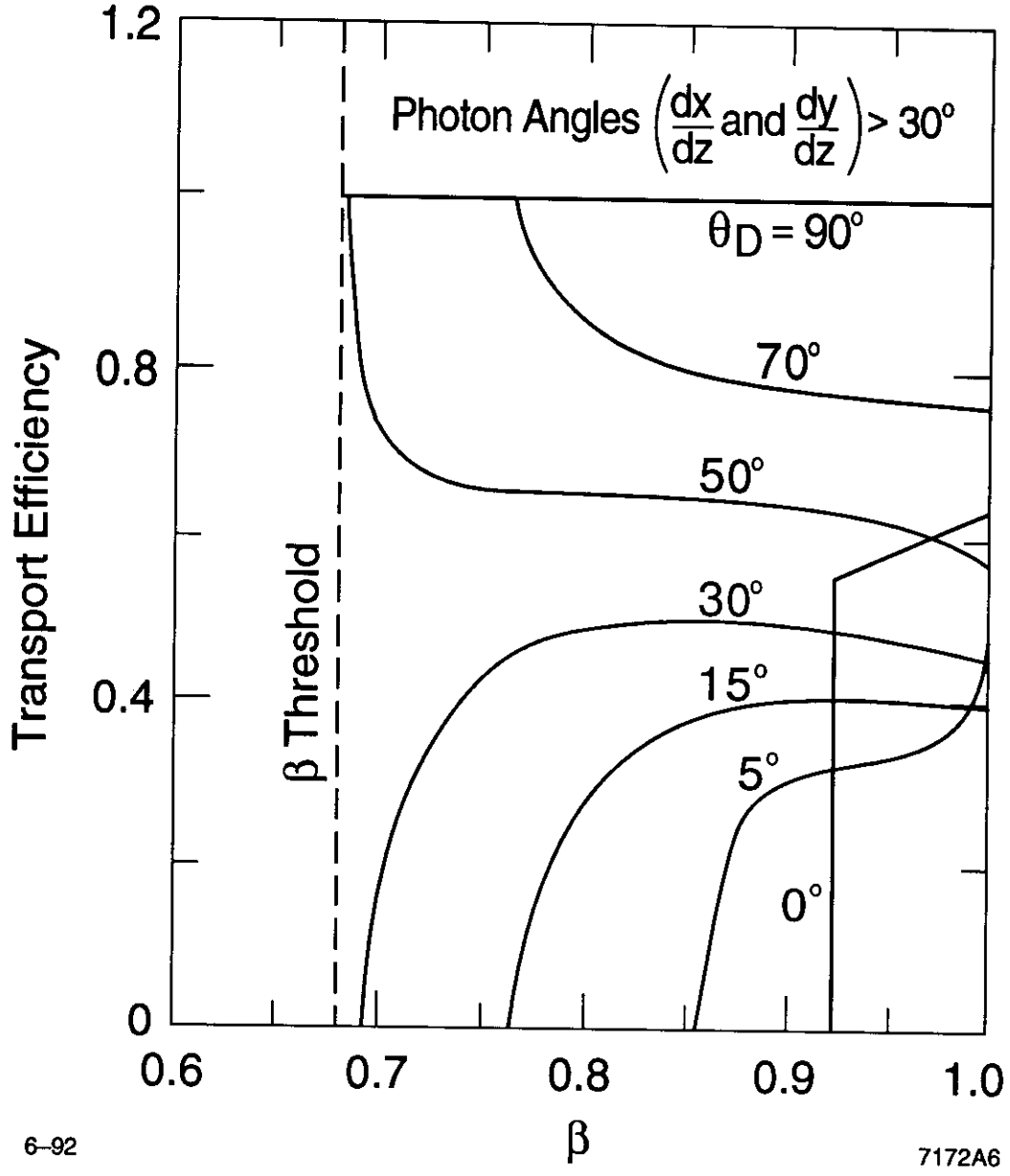

Figure 13. The fraction of Cherenkov photons transmitted to the detector as a function of β with a cutoff in transmission angle with respect to the bar as described in the text.

The number of photoelectrons N_{PE} expected for a $\beta=1$ particle as a function of dip angle is shown in the following table:

Table 1: The number of photoelectrons expected for a $\beta=1$particle as a function of dip angle.

θ_D	N_{PE}
0	27
15	17
30	22
50	56
70	83

The total separation in Cherenkov angle $\delta\theta_c$(tot) is given by

$$\delta\theta_c(\text{tot}) = \frac{\delta\theta_c}{\sqrt{N_{PE}}} \quad , \tag{3}$$

where the angular error measurement from each photon detected $\delta\theta_c$ is

$$\delta\theta_c = \sqrt{\delta\theta^2_{\text{Production}} + \delta\theta^2_{\text{Transport}} + \delta\theta^2_{\text{Detection}}} \tag{4}$$

7.1 $\delta\theta_{\text{Production}}$

Each of these terms include a number of contributions. The error associated with the Cherenkov photon production process $\delta\theta_{\text{Production}}$ is dominated by chromatic dispersion $\delta\theta_{\text{Chromatic}}$, and also includes contributions from multiple scattering $\delta\theta_{MS}$, and momentum bending in the radiator, $\delta\theta_{\text{Momentum}}$. Dispersion in the radiator is the "fundamental" performance limit on attainable performance in an imaging Cherenkov. It is given by

$$\delta\theta_{\text{Chromatic}} = \frac{1}{\tan\theta_c}\frac{dn}{n} \quad . \tag{5}$$

Thus, the chromatic dispersion contribution depends on the radiator dispersion averaged over the response of the photodetector. For a DIRC with a quartz radiator and bialkali photocathodes, this averaged value of $\frac{dn}{n}$ is 5.8 mr, so that $\delta\theta_{\text{Chromatic}}$ is 5.4 mr for a $\beta=1$ particle.

The error associated with multiple scattering $\delta\theta_{MS}$ is quite small and is dominated by angular scattering in the radiator. For a track at perpendicular incidence,

$$\delta\theta_{\text{Multiple Scattering}} \approx \frac{3.1mr}{P(GeV)} \quad . \qquad (6)$$

There is also a smearing in the production Cherenkov angle due to the bending of the particle trajectory in the radiator. This contribution is quite small since the radiator is thin and the bending is approximately in the x, y plane. Its maximum value for a detector in a 1T field is given by

$$\delta\theta_{\text{Momentum}}(max) = 3x10^{-4}\frac{BL}{P\sqrt{12}} = \frac{1.1\text{mr}}{P(GeV/c)} \quad , \qquad (7)$$

and can be ignored.

7.2 $\delta\theta_{Production}$

The smearing of the Cherenkov photons in transport $\delta\theta_{\text{Transport}}$ along the radiator bars is a function of a number of mechanisms. Some of these (e.g., small non-parallelism of the surfaces or a small number of well defined changes in bar angle) can be calibrated out, in principle. Others (such as surface "waves" or variations in refractive index) could lead to emittance growth and must be strictly controlled. Figure and surface quality specifications typical of optical components would be more than adequate. For example, a typical optical flat has a surface figure of about $1/8\lambda$, nearly three orders of magnitude better than these bars would require. Thus, the problem is not so much of principle, but rather economics. For the smearing calculation here, it will be assumed that quality can be sufficiently well controlled that $\delta\theta_{\text{Transport}}$ can be ignored.

7.3 $\delta\theta_{Detector}$

The smearing of the photon angles due to measurement granularity comes from the size of the Cherenkov image (as formed by the bar dimensions) convoluted with the granularity of the photodetector surface, divided by the length from the radiator end to the detector. It is not "fundamental" but is driven by economics. For example, for a photon traveling in the y-z

plane, if we assume a detector made up of closely packed 2 in. PMTs (with spatial resolution δy_{PMT}) located at 165 cm (L) from the end of the 1.23 cm thick radiator,

$$\delta\theta_{Detector} \approx \sqrt{\left(\frac{\delta y^2_{PMT} + \delta y^2_{radiator}}{L^2}\right)} = 6.8mr \qquad (8)$$

7.4 Performance

The performance of any imaging Cherenkov is a strong function of momentum, of course, because the angular separation between particle species is such a rapidly varying function of momentum, as shown in Fig. 14. The solid line compares these differences to the resolution performance expected for a counter of the type described above for a track at a 30 degree dip angle.The e/π separation is quite good to above 1 GeV/c, and π/K separation to about 4 GeV/c. The device has excellent K/p separation well above 5 GeV/c, although it does not turn on for some lab angles for momenta below 1.24 GeV/c

The expected π/K separation versus momentum is shown in Fig. 15. There is a natural enhancement of the separation at the forward angles due primarily to the increasing number of photons detected. Since the asymmetric machines can only produce the fastest particles at large dip angles, the detector described above actually has over 5σ separation for all B Factory tracks.

8. COMMENTS ON THE DETECTOR MODEL

A few comments follow on choices made in the model detector and some possible changes to the model:

8.1 Penetration of the Magnet Poles Pieces

The solution discussed above requires very high quality radiator bars since much of the light will initially be traveling the "wrong" way, and needs to be reflected from the non-readout end and travel down the entire bar. It also needs full detectors at each end which may lead to unacceptable costs. The space to iron ratio at the penetrations in this model are 1 to 1. It is not clear without a more detailed magnetic field study how this would affect the field.

There are many other options for penetrating the magnet pole pieces which can be considered, but all have some potential difficulties, and require understanding the magnet design in more detail. For example, a related option would be to block the bars azimuthally by pole iron over some fraction of their width, and perhaps, compensate the lost light by increasing radiator thickness, at the cost of increasing the radiation length for the particles which travel through the blocked bars. This solution could utilize either single or double

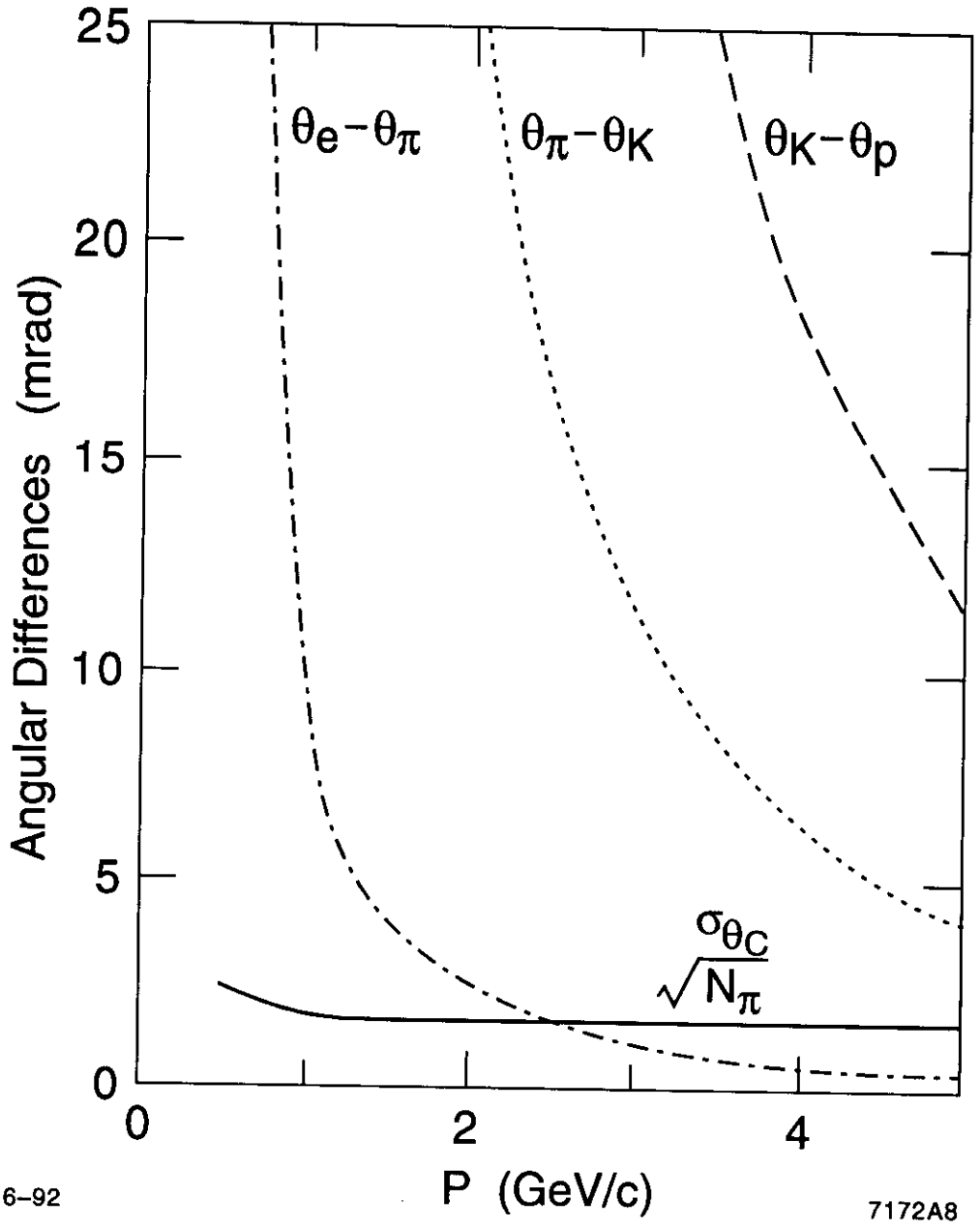

Figure 14. A comparison of the angular differences between various pairs of particles as a function of momentum. The solid line compares these differences to the resolution performance expected for a counter of the type described in the text for a track at a 30° dip angle.

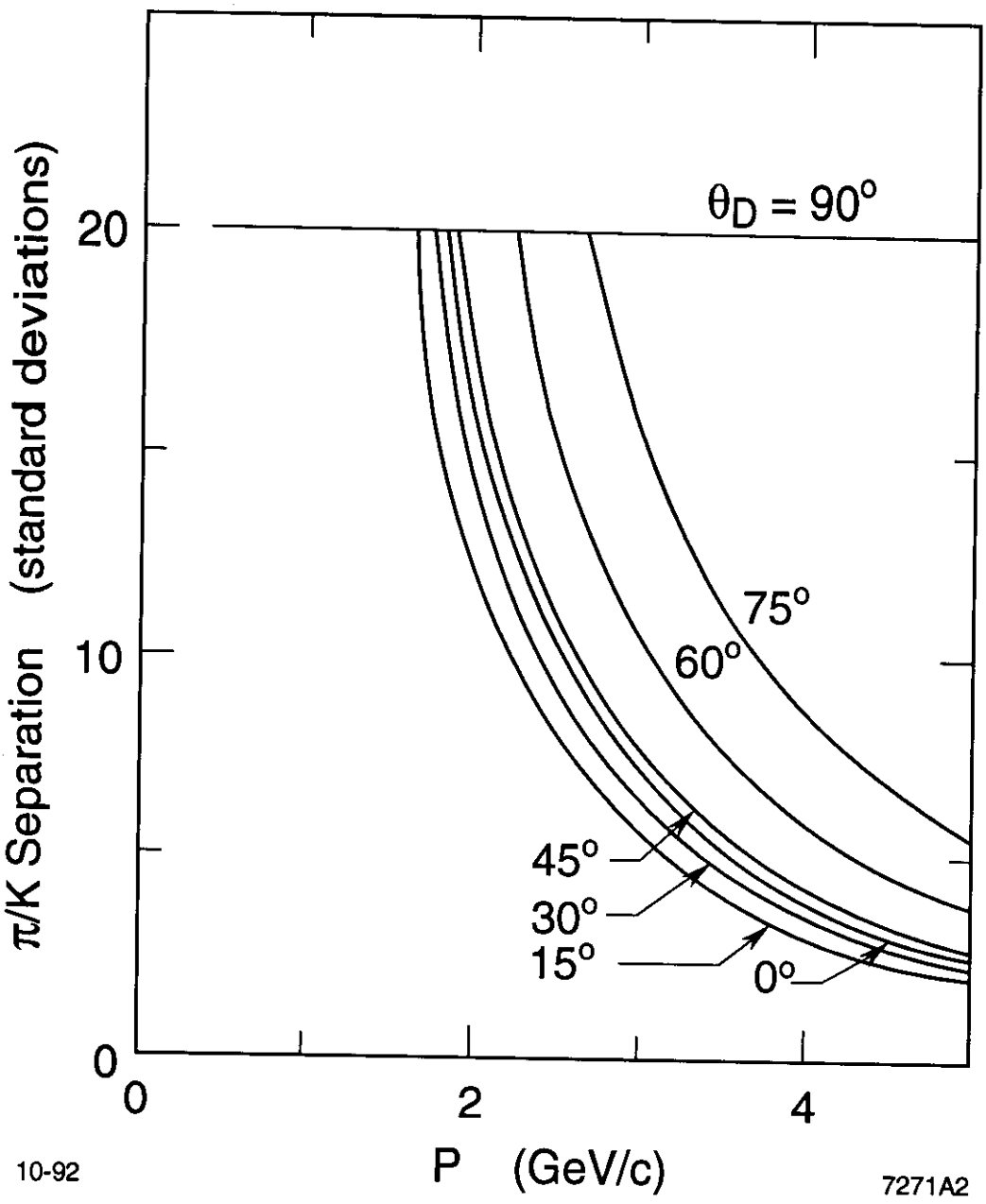

Figure 15. The predicted π/K separation as a function of momentum in a DIRC counter with a detector resolution of 6.8 mr. The lines show the dependence for a variety of track dip angles θ_D.

ended readout. It is unclear how much of the azimuth would need to be blocked to attain sufficient strength from the pole pieces.

A third option is to bend the bars outward radially so that the penetration occurs at a larger radius. The amount of space gained is a function of the geometry, but any bend will create imaging doubling (and pattern confusion), and, for many angles, a fraction of the photons will be lost.

The nicest "theoretical" option (from a DIRC perspective) with tubes outside the field is to design the pole pieces with full penetrations azimuthally, and with external supports (probably to outer return iron). In this case, the photodetection surface would lie inside the support structure. Such a magnet design is certainly unusual and needs engineering design.

Finally, the best solution of all would be to find photodetectors with adequate performance that would operate in a magnetic field.

8.2 Endcaps

The endcap-less detector configuration described above creates a very uniform device for the entire detector and avoids the problems created by particles penetrating the central tracking endplates, but it does lead to long detectors. In particular, it may be difficult to construct such a long, low-mass tracking chamber. The effective radiation length in front of the calorimeter is also a rather rapid function of dip angle near the detector ends which will tend to reduce the performance of the calorimeter there. For example, with a radiator whose nominal thickness is 10% L_{RAD}, the actual thickness is 31% L_{RAD} at the maximum dip angle of 71.8° ($\cos \theta_D = 0.95$), and exceeds 20% L_{RAD} over 8.4% of the solid angle. If present detectors are any guide, it seems quite unlikely that a detector with endcaps could beat or even come close to equalling this, but it is possible to build a DIRC with an endcap if it were required. Since light is lost going around a bend, it might need to be somewhat thicker than the barrel device for equal performance, and the combined light bars at the magnet poles would be significantly thicker.

8.3 Detector Issues

The number of PMTs required for a DIRC is large and a major component of the cost. Essentially, the detector resolution specification "fixes" the number of pixels required to cover a certain solid angle. Pixels must be placed sufficiently far away from the radiator end to reach the required resolution, and, in the limit that the bar size is negligible, and the detectors for neighboring bars do not overlap, the number of pixels required for each single bar device is an invariant. The size required for these pixels is dependent on the nature of the focusing system. For the non-focusing "proximity" system discussed above, there is a simple relationship between pixel size and the distance between the radiator end and the detector surface. Focusing systems could in principle make use of smaller pixels, and reduce the apparent size of the radiator bar, as discussed below. In the device described above, there is substantial overlap of coverage azimuthally, so that the number of required pixels actually grows rather rapidly as the pixel size shrinks. Figure 16 shows the number of

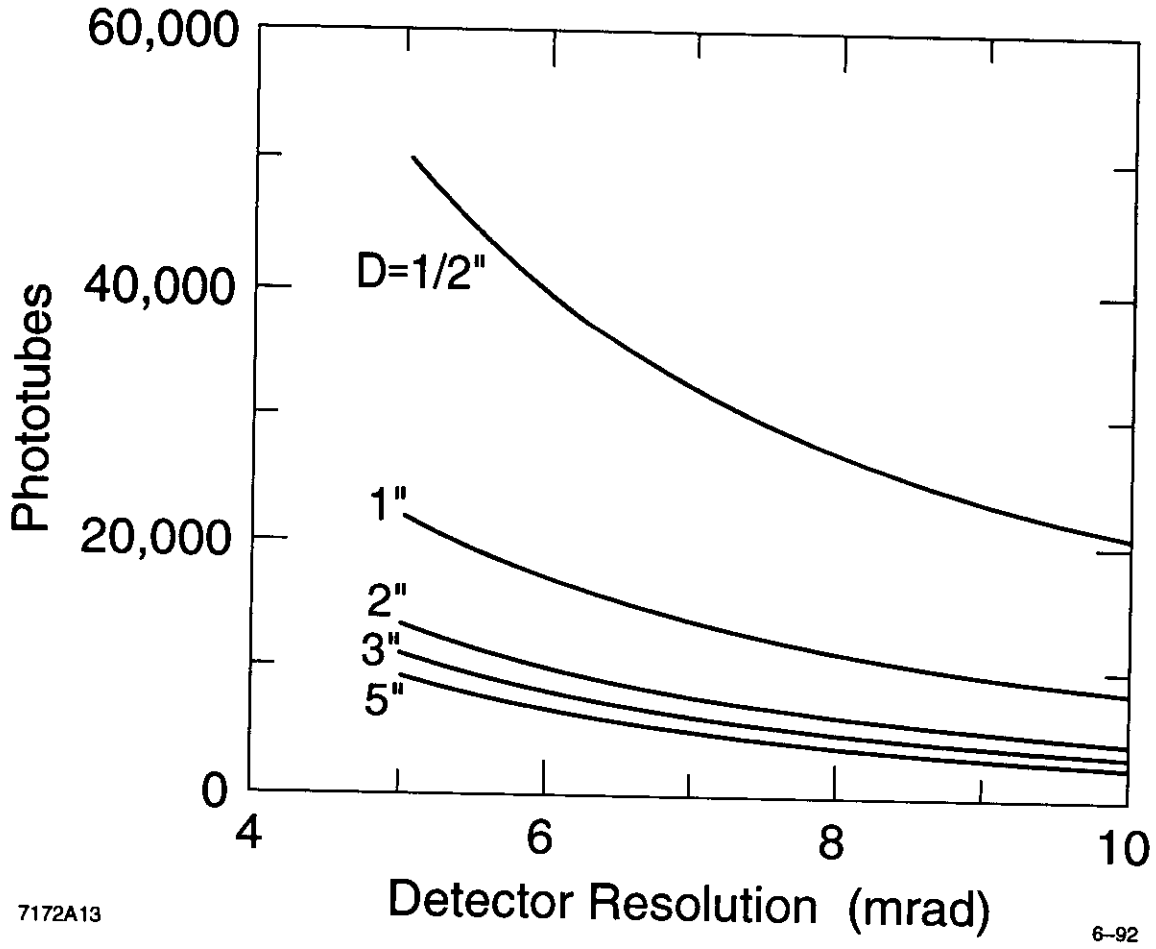

Figure 16. The number of PMTs required per readout end versus resolution for a variety of different phototube diameters.

PMTs required at each detector end in the model above as a function of desired detector resolution. Of course, resolution is not the only relevant concern. In general, a device with more pixels has better multi-track separation and fewer ambiguities. Minimization of the detector cost, while keeping the track overlap problem under control, tends to lead to tubes in the 2 in. range. For a particular PMT size and detector geometry, there are a number of possible ways to reduce the number of tubes, but all have performance implications. In the device described above, it has already been assumed that tube numbers are reduced by using reflection at plane mirrors in the detector boxes. Though this clearly reduces the cost of the detector, it also loses some light, introduces ambiguities, and reduces signal to background. None of these problems is thought to be serious, but further Monte Carlo study is warranted. As discussed above, it is also possible to reduce the number of tubes by reading out the device at only one end. The performance concerns are similar, and it interacts with the choice of magnet door penetration. It is, however, quite attractive conceptually to imagine reading out the device only on the low momentum side, where the angular coverage does not need to extend to low laboratory angles. Unfortunately, this means that Cherenkov photons from the high momentum tracks, which make the most severe demands on the detector, will also travel a long way down the bar, and the performance will suffer unless the bars are very good. A less extreme version of the single ended readout approach is to make use of the inherent asymmetry, and make detectors with different resolutions on the forward and backward ends. Finally, if very fast tubes could be used, the measurement of angle from the time dimension may become competitive with that available from position. This might allow a design with lesser resolution in one or both of the position measurements. Alternatively, in a high background environment, excellent time resolution will lead to better background rejection.

In principle, a focusing system can be devised which will compensate for the finite size of the detector bar. This might allow the use of a rather small detection surface, with significantly smaller pixel size. The azimuthally close packing, the very wide azimuthal acceptance, and the need for geometric and chromatic correction makes this difficult particularly in the azimuthal direction, and limits the focusing that can be attained in practice, but further Monte Carlo studies are of interest to see how small the detector could be made, and what the demands on such a detector would be. This would be of particular interest if the photodetection surface could be placed inside the magnet, and/or were made of silicon.

Finally, there are other mechanisms for obtaining information on the photon angle other than the standoff proximity focusing scheme discussed here.[14] Some of these schemes are conceptually attractive and should be considered more carefully.

8.4 Costs

The cost optimization of a DIRC is a complex multiparameter problem, and depends on many of the design choices just discussed. In general, radiator thickness can be traded for tube performance or radiator quality, and the number of channels can be traded against per-channel cost and desired performance. Although radiator issues are probably the least

well understood technically, the cost is almost certainly dominated by per-channel detection and readout costs. As a very rough guess, the model device discussed above would probably cost about 10–12 M$. Possible cost savings include: 1) single ended readout to save phototubes, 2) cheaper phototubes (e.g., from FSU sources), 3) improved HV and readout system design, 4) accepting somewhat worse resolution performance, 5) accepting somewhat more material in the detector. In particular, a device with a 10 mr $\delta\theta_{Detector}$ would cost about 60% of the device discussed above and would still have around 4 σ π/K separation or better at all B factory momenta as shown in Fig. 17. Finally, it should also be realized that space inside a crystal calorimeter is extremely expensive. For example, if a DIRC saves 15 cm of space which allows a smaller calorimeter, the cost savings would be in the 6–10 M$ range. In this sense the DIRC might be said to "pay for itself."

9. CONCLUSION

The DIRC has many attractive features and appears to be extremely well matched to the requirements for a particle identification device at the B factory. Of course, there are a number of potential problems that need to be addressed for the DIRC, and since it is a new device, a full scientific prototype is highly desirable. The Cherenkov light must penetrate the magnet end plates to get out of the field and, even some distance from the magnet, shielding the tube array from the field may be troublesome. The number of tubes required is quite large (typically of order 10,000), so the cost will be rather large. The most uncertain elements are the radiator pieces themselves. Though the finish specifications are not particularly severe by optical standards, the pieces are very large and it will be a major challenge to produce them in the sizes required and still keep costs under control. R&D is now centered on radiator production and evaluation, photodetector evaluation and construction, and software studies, leading to the construction and testing of a physics prototype.

REFERENCES

1. See, for example, D. MacFarlane, Proceedings of the International Conference on B Factories: The State of the Art in Accelerators, Detectors and Physics, Stanford, CA, April 6-10,1992.
2. For reviews, see e.g., B. Ratcliff SLAC-PUB-5853(1992), and P. Coyle et. al., SLAC-PUB-5594 (1991).
3. SLAC-REP-373 (1991).
4. See, for example, Particle Identification, Proceedings of the International Conference on B Factories: The State of the Art in Accelerators, Detectors and Physics, Stanford, CA., April 6-10,1992.
5. P. Baillon, NIM A238 (1985) 341; S. Yellin, CRID analysis internal note.
6. For a simple analytic treatment of image formation, see, Blair Ratcliff, Presentation to the PEP-II Particle ID working group, July 1992.

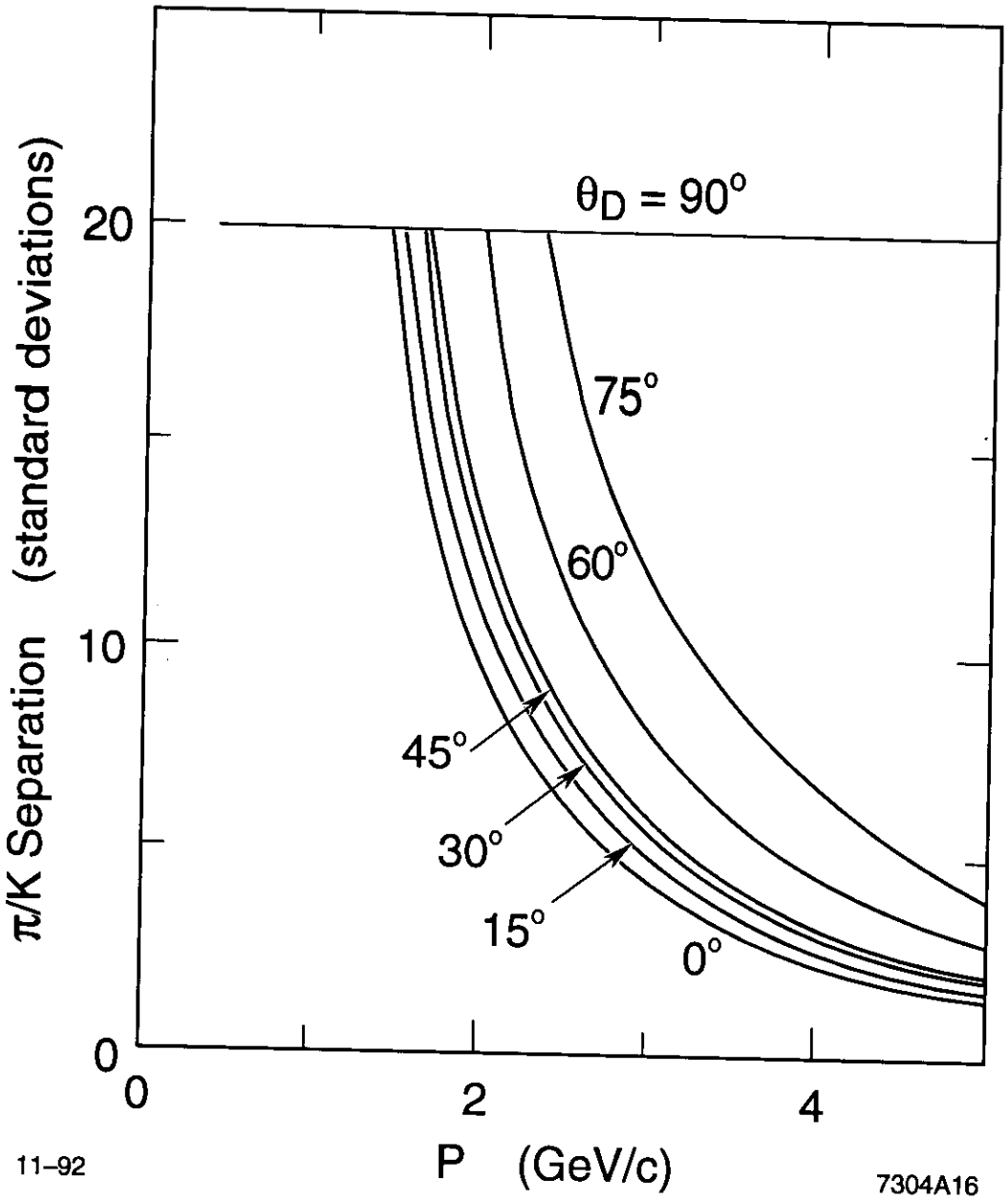

Figure 17. The predicted π/K separation as a function of momentum in a DIRC counter with a detector resolution of 10 mr. The lines show the dependence for a variety of track dip angles θ_D.

7. R.M Bionta et al., Proceedings of the 17th Rencontre de Moriond (1982).
8. G.Kettenring, NIM 131 (1975) 451; manufacturers data, Rohm and Haas, Philadelphia, PA.
9. R.P. Cargille Labs, Cedar Grove NJ, USA.
10. Fiberguide Industries, Stirling NJ, USA.
11. Melles Griot, Irving CA, USA.
12. See, for example, Advanced Photonics, Camarillo, CA.
13. M. Atac et al., Nucl. Instrum. Meth. A320 p. 1255-160 (1992).
14. See, for example, B. Ratcliff in BaBar Note 37, and P. Coyle, Presentation to the PEP-II Particle ID Working group, April 1990.